Journal of Power Sources 365 (2017) 327–338

Contents lists available at ScienceDirect

Journal of Power Sources

journal homepage: www.elsevier.com/locate/jpowsour

Cycling capacity recovery effect: A coulombic efficiency and post-mortem study

Jörn Wilhelm [a, *], Stefan Seidlmayer [b], Peter Keil [a], Jörg Schuster [c], Armin Kriele [d], Ralph Gilles [b], Andreas Jossen [a]

[a] Institute for Electrical Energy Storage Technology (EES), Technical University of Munich (TUM), Arcisstr. 21, 80333, München, Germany
[b] Heinz Maier-Leibnitz Zentrum (MLZ), Technical University of Munich (TUM), Lichtenbergstr. 1, 85748, Garching, Germany
[c] Chair of Technical Electrochemistry, Technical University of Munich (TUM), Lichtenbergstr. 4, 85748, Garching, Germany
[d] German Engineering Materials Science Centre at MLZ, Helmholtz-Zentrum Geesthacht, Lichtenbergstr. 1, 85748, Garching, Germany

HIGHLIGHTS

- Lithiation of anode overhang areas causes reversible capacity increase or decrease.
- XRD and color analysis shows lithiation of large 2–6 cm long overhang regions.
- High storage SoC batteries show CE > 1 and rising capacity during 1200 h of cycling.
- Long term storage can distort SoH assessment.

ARTICLE INFO

Article history:
Received 4 July 2017
Received in revised form
19 August 2017
Accepted 23 August 2017

Keywords:
Lithium-ion battery
Calendar aging
Capacity recovery
Anode overhang
X-ray diffraction
Coulombic efficiency

ABSTRACT

The analysis of lithium-ion battery aging relies on correct differentiation between irreversible and reversible capacity changes. Anode overhang regions have been observed to influence Coulombic Efficiency (CE) measurements through lithium diffusion into and out of these areas, complicating precise capacity determination. This work presents an analysis of the extent of graphite anode overhang lithiation after calendar storage by means of local X-ray diffraction (XRD), CE measurements, and color change analysis. We found LiC_{12} lithiation of the anode overhang area after 20 month storage at 40 °C at high state of charge (SoC) and partial lithiation (LiC_{18}) at medium SoC storage at 40 °C and 25 °C. Graphite color changes in the overhang areas are observed and consistent with the state of lithiation measured by XRD. Coulombic efficiencies greater than unity and increasing capacity during 1200 h of cycling are detected for high SoC storage cells. The capacity difference between high and low storage SoC batteries decreases by up to 40 mAh (3.6% of nominal capacity) after cycling compared to tests directly after storage. Consequently, the size of the anode overhang areas as well as the battery storage temperature and duration need to be considered in CE analysis and state of health assessment.

1. Introduction

Lithium-ion batteries are widely used as energy storage in portable electronics, electro mobility and stationary storage applications. Along with research on new active materials, a key challenge of current investigations is to understand and improve the aging behavior of established battery active materials, such as graphite, $LiFePO_4$, and NMC(111), to achieve a longer and better predictable battery lifetime [1,2].

Two types of studies form the basis for aging experiments; calendar aging experiments where batteries are stored at various conditions for several months or years [3–7], and cycling studies where batteries are repeatedly charged and discharged [8–10], often replicating real use scenarios [11]. These experiments rely on precise capacity measurements to correctly distinguish between irreversible effects, such as loss of cyclable lithium, and reversible effects, such as temperature dependent rate capability. New ultra-high precision coulombic efficiency experiments may reduce the need for costly long term measurements through early detection of side reactions and better predictability of battery lifetime [12,13].

* Corresponding author.
E-mail address: joern.wilhelm@tum.de (J. Wilhelm).

http://dx.doi.org/10.1016/j.jpowsour.2017.08.090
0378-7753/

The changes in CE due to degradation processes through parasitic reactions are very small. Thus, CE studies of these processes require precisely set currents, high precision voltage measurements as well as strictly controlled sample environments [14].

The high sensitivity of these measurements under controlled sample conditions led to the discovery of a surprising reversible capacity effect. Studies found "anomalous transient CEs" with CE > 1 in high precision cycling experiments after storage [15,16]. This behavior was linked to anode "overhang", acting as a lithium-ion source or sink depending on the charging or discharging scenario [16]. Anode overhang means, that areas of the anode active material do not have a cathode counterpart. This results from the negative electrode in a lithium-ion cell being designed slightly larger than the positive electrode. This is a common design feature to assure 100% cathode-anode overlap and to avoid lithium plating at the border area of the graphite anode [17]. The analysis of 220 mAh wound pouch bag cells with 1 mm side overhangs showed a lithiation of the overhang regions after high SoC storage. Previous studies determined that the storage SoC affected the CE for up to 1000 h of subsequent cycling [16]. Reversible and SoC-depending capacity increase was also observed by Lewerenz et al., who performed calendar and cyclic aging experiments with 8 Ah cylindrical cells at elevated temperatures [18]. They also attribute this effect to anode overhang areas.

To study the effects of large overhang areas in more detail, we examined cylindrical lithium-ion cells which feature wide overhang areas of 2–6 cm in addition to smaller side overhang areas of 1.5 mm.

These areas without cathode counterpart are located at the innermost and outermost winding of the jelly roll (Fig. 1b). They are ionically connected to the lithium electrolyte reservoir. Given the slow lithium diffusion processes in batteries – can these wide areas be lithiated and influence CE and capacity measurements in commercial cells? To examine this, we performed CE and post-mortem analyses of commercial cylindrical cells after long term storage at SoCs ranging from 0% to 100%.

The post-mortem analysis consists of a qualitative assessment of the overhang area through observation of color changes complemented by ex-situ XRD for quantitative local information.

Graphite shows a well-known color change upon intercalation of lithium. We use this to detect lithium transport into the overhang regions. A fully lithiated LiC_6 graphite is golden. With decreasing amount of LiC_6 in a LiC_6/LiC_{12} mixture, the color changes from golden to golden-brown to reddish-brown. At lower lithiated states, the color changes over blue-grey to a metallic dark grey [19–21].

XRD can be applied to detect SoC inhomogeneity in electrodes [22]. We extend this to the graphite overhang area. XRD measurements complement the color analysis as the X-rays penetrate the electrode layer and active material particles. The resulting diffraction pattern contains the structural information of the exposed volume. In contrast, in a top view image of an extracted electrode only the surface of the graphite particles at the surface of the electrode layer is visible. The observed surface lithiation differs from the average electrode lithiation if lithiation gradients within particles or the layer are present [21].

In this publication, we qualitatively and quantitatively investigate the lithium diffusion into graphite anode overhang sections with local X-ray diffraction, high precision coulometry and post-mortem color analysis to assess the overhang region's impact on

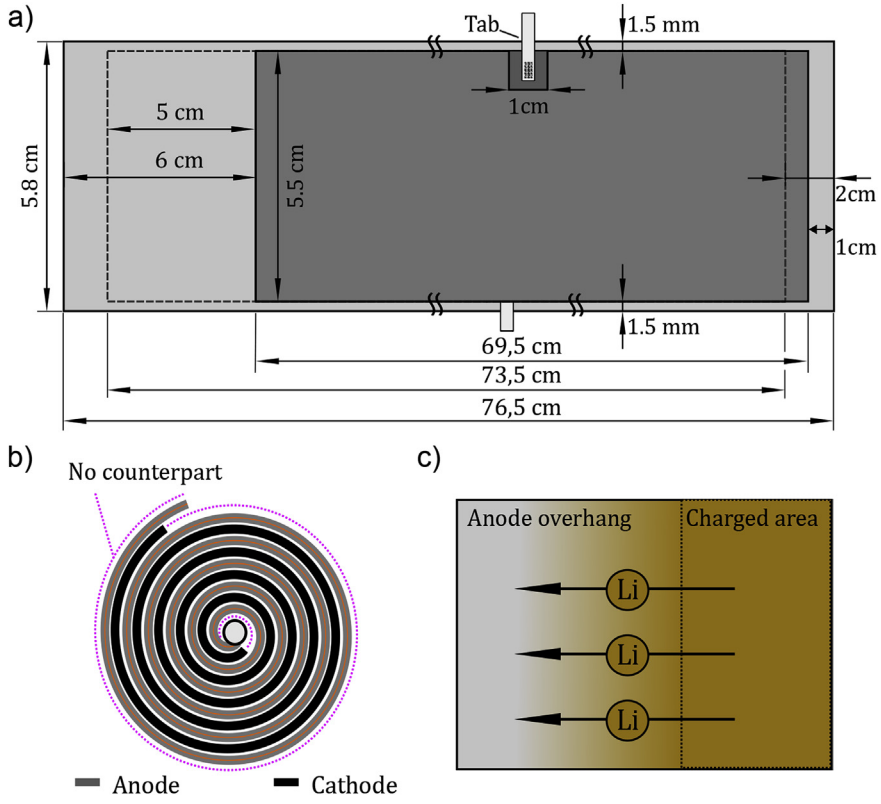

Fig. 1. a) Schematic layout of the anode electrode area of sample cells with cathode counterpart (dark grey) and without cathode counterpart (light grey). The dashed lines show the cathode covered area on the flipside of the electrode. b) Schematic of a cylindrical cell's jelly roll consisting of anode, cathode and separator (not shown). The overhang areas are highlighted (pink). c) Schematic of the lithium diffusion process from a charged anode area (golden) to an uncharged overhang area (grey). (For interpretation of the references to colour in this figure legend, the reader is referred to the web version of this article.)

capacity measurements and state of health (SoH) determination.

2. Experimental

We investigated the commercial $LiFePO_4$|graphite battery cells of type A123 APR18650M1A. The graphite anode of this cylindrical cell type battery exhibits large overhang regions and excellent electrode stability, which aids sample preparation after battery disassembly. Further battery properties are listed in Table 1.

2.1. Electrode geometry

A schematic of the electrode geometry is shown in Fig. 1. The anode width is 58 mm and cathode width is 55 mm. The anode overhang is thus 1.5 mm at each side if the electrodes are ideally positioned. The cathode is considerably shorter (71.4 cm) than the anode (76.5 cm). Both, the anode and the cathode, are fully double-sided coated. The excess in length of the anode leads to overhang areas at the outermost and innermost part of the jelly roll as depicted in Fig. 1a) and b). The two largest overhang areas consist of a 2.0×5.8 cm^2 inactive region at the inner end and 6×5.8 cm^2 at the outer end of the anode coil. These overhang areas represent 5.2% of the total anode area. The thin overhang area 68.5×0.3 cm^2 corresponds to 4.6%. Together they represent about 10% of the total anode area. The length of the cathode covered area marked in Fig. 1 for the front (73.5 cm) and back (69.5 cm) is different from each other and from the length of the cathode (71.4 cm). This is due to the spiral winding of the electrodes in the jelly roll.

The anode and the cathode are connected by a single tab, centered at the electrode in close proximity. The tab area is about 1 cm^2 and the opposing electrode at this position does not have an active material counterpart similar to the overhang regions.

2.2. Calendar aging

As part of a calendar aging study, 16 batteries were stored at 40 °C for 20 months at different SoCs. The SoC range examined in the experiment covers 0–100% SoC in 10% steps with additional steps at 5%, 45%, 55%, 65% and 95% for higher resolution. In the following, the SoC is defined with respect to the actual cell capacity C_{actual}:

$$SoC = \frac{Q_{stored}}{C_{actual}}$$

To assess the SoH, the batteries underwent a periodic check up procedure to determine actual capacity, to perform differential voltage analysis (DVA) and to identify changes in the battery resistance. The check up procedure was carried out at 25 °C every 2–4 months with a higher frequency of tests at the beginning of the storage experiment. For a detailed description of the calendar aging setup and measurements, the reader is referred to [3]. Additionally, two batteries stored at 50% SoC and 25 °C for 20 months were included to study lithiation into overhang areas at room temperature. An additional battery was investigated as reference for the balancing measurement of a fully charged graphite electrode. For this purpose, the battery was charged to 100% SoC using a constant current constant voltage (CCCV) procedure (3.6 V, 100 mA, I < 0.01CA).

All samples are listed in Table 2 with their corresponding identifiers. The identifier (Id) is composed of *S*-Storage, *CV*-Constant voltage and the storage SoC (SoC_{actual}). For batteries stored at 25 °C the temperature value *25* is added. Furthermore, Table 2 lists the state the samples are stored at after the last check up in absolute values C_{actual} and with reference to the initial capacity $SoC_{initial}$.

2.3. Test procedure

The SoC dependency of diffusion into large overhang areas was studied with three cells stored for 20 months at elevated temperature (40 °C) and high (95%), medium (55%), and low SoC (0%). These samples S95, S55, and S00 were opened, the electrodes extracted, washed and prepared for photo and XRD. Pictures were taken of the graphite color distribution at the thin side overhang regions as well as large overhang regions, cathode tab covered areas and active electrode area. X-ray diffraction measurements for sample S95 were performed at 20 positions along the electrode length up to the central tab location and 11 positions across the width of the electrode. An additional sample S50-25, was stored at 50% SoC and room temperature (25 °C) to study diffusion into large overhang areas during long term storage at realistic storage conditions. As with S95, S55, and S00, the graphite color distribution was photographed and the graphite phase fraction measured in the largest overhang region. To see whether lithium diffusion out of and into the overhang area during storage affects the battery cycling, we performed high precision CE measurements with samples S05, S10, S20, S40, S60, S80, S90 and S100. Constant current cycling was performed with 250 mA (~C/4) at 25 °C with 10 min resting periods between charging and discharging. The batteries were cycled between 2.5 V and 3.6 V.

After 30 cycles (~250 h), cycling is ended for samples S05, S60, S70, S90, and S100 after discharge. Sample S90 was disassembled within 2 h. To further deplete the overhang lithium reservoir, the samples S05, S60, S70, and S100 were then stored at 0% SoC and 50 °C for 50 h. Every 10 h, the samples were discharged CCCV to 2.5 V (I = 100 mA, I < 0.01CA). After this procedure, the samples were disassembled, photographed and XRD measurements taken. CE measurements were continued up to 300 cycles (2000 h) for S10, S20, S40, and S80.

2.4. Post-mortem

The cells were disassembled in a glovebox with O_2 and H_2O removal in argon atmosphere (MBRAUN; <1 ppm H_2O & <1 ppm O_2). The metal casing was cut open, anode, cathode and separator were extracted and separated. The electrodes were washed with dimethyl carbonate (DMC) for 20 min to remove electrolyte remnants. The electrodes were then dried at vacuum. Photos were taken before the electrodes were cut and packaged for XRD in PP/PE coated aluminum foil sealed at 50 mbar vacuum and 190 °C.

Table 1
Battery properties.

Manufacturer	A123	Active material	Graphite| $LiFePO_4$
Model	APR18650M1A	Max./min. voltage	3.6 V/2.0 V
Nominal capacity	1.1 Ah	Max. cont. current	+4 A/−30 A
Mass	39 g	Areal capacity	1.4 mAh cm^{-2}
Anode coated area	2×76.5 cm x 5.8 cm = 887 cm^2	Cathode coated area	2×71.4 cm x 5.5 cm = 785 cm^2

2.5. Coulombic-efficiency-setup

Cycling was performed with a BaSyTec CTS battery test system. All tests were conducted at a controlled temperature 25 ± 0.1 °C using a BINDER KT170 climate chamber. For the coulombic efficiency measurements, additional 20 mΩ shunts were placed in the current path between the battery test system and the battery cells. The voltage drop across each shut were measured with an ultra-low noise, 24-bit sigma-delta analog-digital converter from Analog Devices (7193 CE). This enabled the measurement of the currents flowing into and out of each battery cell with a higher resolution and precision than the battery test system. These current data were recorded synchronously by the battery test system. To minimize temperature influences on the measurements, the analog-digital converter board and the shunts were also placed inside the climate chamber at 25 °C to improve the accuracy of CE measurements as recommended in literature [23]. The battery surface temperature was measured with an NTC temperature sensor attached to the battery. The observed change in surface temperature during cycling was <0.5 °C.

2.6. Color-setup

Images of washed and dried electrodes were taken with a SONY Alpha 7 II camera with a Sony FE 55 mm F1.8 ZA objective. The images were taken at a fixed sample, camera and lighting position. Photos are taken from outside the glovebox with the samples being inside the glovebox, at a lithiated state. The color representation is expected to be distorted due to absorption of the glovebox glass window and the internal camera color calibration. To get an accurate representation of the electrode colors, we performed white balancing and color calibration with each image using datacolor SpyderCheckr 24 color reference cards placed inside the glovebox together with the samples. For better visibility of color gradients, brightness is slightly increased for the electrode images in this paper and the supplementary files (Figs. S3–S14). Image correction was performed with Adobe Photoshop Lightroom v5.7.1, Adobe Camera Raw 8.7.1 and SpyderCheckr v1.2.2.

2.7. XRD-setup

Diffraction analysis was performed with a PANalytical Empyrean™ X-ray diffractometer in the Materials Science Laboratory of Heinz Maier-Leibnitz Zentrum using Mo-$K_{\alpha 1}$ radiation at $\lambda = 0.70932$ Å, 55 kV and 40 mA. The sealed electrodes were placed in the center of the goniometer circle (radius 240 mm) and were measured in transmission mode which requires a high X-ray beam intensity realized by a focusing mirror. Hence an elliptic graded W/Si multilayer mirror with an equatorial divergence of the beam less than 0.055° was used to collimate the divergent beam from the X-ray tube to the secondary focus of the goniometer circle at the detector. A 1D real time multistrip X'Celerator™ detector with an efficiency of 30% for Mo Kα1 radiation and a pixel resolution of 0.002° in 2θ was used to collect the data. The Mo K_β radiation is suppressed to a level below 0.5% by the focusing mirror.

The axial divergence was reduced by inserting Soller slits with an opening of 0.02 rad at the incident and transmitted beam path. The beam cross section at the sample was reduced to 10 mm × 0.38 mm using masks and a 1/4° Ta divergence slit.

For standard measurements, 4–16 patterns were collected typically over a 2θ-range of 7–37° with a step size of 0.008° and a counting time per step of 36.8 s. Long term measurements used up to 170 patterns with a 2θ-range of 5°–55°. The sealed electrodes were mounted on a sample holder and were kept perpendicular with respect to the incident beam during measurement. The sample position was adjusted manually with a positional resolution of 0.5 mm.

The refinements were carried out using the Highscore software package [24] with Thomson-Cox-Hastings (TCH) type [25] pseudo-Voigt profile functions either as Rietveld [26] or Pawley [27] fit, as implemented in the software. All refinements were carried out starting with the reference data sets for Al [28], Cu [29], Graphite [30], LiC_{12} [31] and LiC_6 [32] from the Inorganic Crystal Structure Database (ICSD) maintained by the FIZ Karlsruhe. The reference data sets as well as the fitting parameters, including standard uncertainties for all measurements, are tabled in the supplementary material (Tables S1–S7).

2.8. XRD-analysis

Our samples also contain lower lithiated structures than the crystallographically established LiC_{12} phase. The transition from graphite to LiC_{12} is subject to long-standing discussion. According to the established staging model, the structural change follows: C (graphite) ↔ stage 4L (LiC_{24}) ↔ stage 3L (LiC_{18}) stage 2 (LiC_{12}) [33–35]. Recent publications suggest an alternative mechanism with up to seven higher order phases (Phase IIL – Phase XXVIIIpp) as a result of modulation within ab-planes of graphite layers ("twisted bilayer behavior"), instead of the layer ordering of the staging model [36]. Given the limited resolution and angular range of our data as well as continuing discussion on the transition mechanism, we adopt a simplified picture of lower lithiated phases. Lower lithiated phases are classified qualitatively according to the shift of the c-axis. Phases with shifted c-axes below 7.040 Å are considered as LiC_{18}. Phases with shifted c-axes below 6.900 Å are considered as $LiC_{\geq 24}$.

2.9. Pattern-shift due to coating position

Anode and cathode electrodes are coated on both sides of the current collector (CC). Each side is penetrated by the X-ray beam and contributes to the diffraction pattern. The relative displacement of the active material layers due to the current collector is ~15 μm. The total thickness of a double coated electrode and thus the upper displacement limit for two graphite particles is ~90 μm. A simulation of the LiC_6, LiC_{12}, and graphite 002 reflections for two positions shifted by 100 μm in X-ray beam direction shows a resulting shift of 0.005°2θ (see also Supplementary Fig. S1). The resulting shift is below the 0.008° step size of the diffractometer and thus negligible for 100 μm displacement. The specimen displacement between different samples after replacement is corrected with the Cu reflection of the current collector.

3. Results and discussion

3.1. Calendar aging

To analyze the diffusion of lithium into the graphite electrode overhang regions, it has to be taken into account that due to calendar aging, the amount of usable lithium and thus achievable lithiation is reduced. Fig. 2 a) shows the reconstruction of the full cell voltage of a new battery and the differential voltage spectrum from the half cell data plotted versus full cell SoC b). At 100% full cell SoC, the anode capacity is only utilized up to 80%. The dV/dQ maximum at 70% SoC marks the change from the LiC_{12} plateau and the LiC_{12}/LiC_6 graphite voltage plateau. At the given battery balancing, a maximum lithiation of 57% LiC_{12} and 43% LiC_6 in the XRD is expected for a fully charged new battery. Fig. 2 c) shows the capacity decrease during 16.3 months calendar aging at 40 °C. The capacity fade increases with storage SoC. At 0–30% SoC, the losses

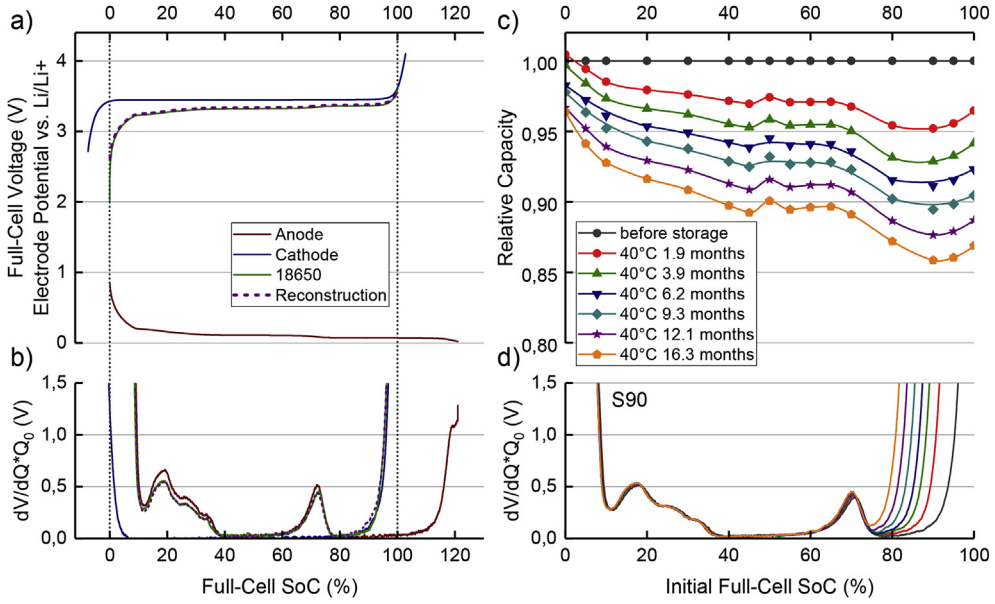

Fig. 2. a), b) Full-cell voltage reconstruction from half cell profiles. c) Capacity fade at 40 °C during calendar aging over storage SoC. d) Differential voltage profile for different stages in the aging process for the battery with the highest relative capacity losses (S90).

are below 10%, at 40–70% the capacity loss is about 10% and up to 14% at 80–100% SoC. The observed plateaus of capacity fade correspond to graphite stages [3]. Fig. 2 d) shows the changes in the differential voltage spectrum for the battery with the highest capacity loss (S90) resulting from calendar aging at 40 °C. A comparison between the capacity and the R_{1kHz} resistance at initial measurements and after 16.3 months storage is given in Table 2. Battery resistances of all samples increased by less than 20% R_{1kHz}. The homogeneous resistance increase indicates that there is no direct correlation between capacity fade and resistance increase. Electrode dry out was not observed as stored and new reference batteries showed visibly wet electrodes and separators during disassembly.

3.2. Coulombic efficiency

When diffusion into or out of overhang areas changes the amount of lithium available for cycling, the coulombic efficiency is affected. To study this, the cells S05, S10, S20, S40, S60, S80, S90, and S100 were cycled and the battery capacity measured. High CE values very close to unity during long-term cycling of up to 1200 h confirm the excellent cycling stability of the examined LFP cells. Thus, no notable aging reactions have occurred which deteriorate the CE measurements.

Fig. 3 demonstrates that there is a strong correlation between the storage SoC and the CE values: The batteries stored at high SoCs of 80%, 90%, and 100% exhibit CE values greater than unity. This means that a slightly higher amount of charge is extracted during

Table 2
Battery Aging Data. Capacity loss and resistance increase during 20 month storage at temperature $T_{storage}$. The capacity loss $\Delta C_{initial\text{-}last}$ is given as difference between the first check up $C_{initial}$ and last check up C_{last} after 16.3 month of storage. The battery resistance is measured at 1 kHz, a temperature of 25 °C and a SoC of 50% during the check up procedure. $R_{last}/R_{initial}$ describes the resistance increase between first and last check up. C_{actual} is the capacity the samples are stored at after the last check up. SoC_{actual} is the corresponding state of charge with reference to the current capacity, $SoC_{initial}$ with reference to the initial capacity $SoC_{initial} = \frac{Q_{stored}}{C_{initial}}$.

Sample	$C_{initial}$	C_{last}	$\Delta C_{initial\text{-}last}$	$R_{initial}$	R_{last}	$R_{last}/R_{initial}$	$SoC_{initial}$	SoC_{actual}	C_{actual}	$T_{storage}$
Id	Ah	Ah	Ah	mΩ	mΩ		%	%	Ah	°C
S00	1.056	1.018	0.038	15.149	17.223	1.14	0	0	0.000	40
S05	1.065	1.002	0.063	15.387	16.973	1.10	5	5	0.050	40
S10	1.068	0.991	0.077	15.347	17.954	1.17	9	10	0.099	40
S20	1.061	0.972	0.089	15.471	18.229	1.18	18	20	0.194	40
S30	1.066	0.969	0.097	15.131	17.521	1.16	27	30	0.291	40
S40	1.073	0.963	0.110	15.210	17.521	1.15	36	40	0.385	40
S45	1.053	0.940	0.113	15.040	17.909	1.19	40	45	0.423	40
S50	1.067	0.961	0.106	15.235	18.216	1.20	45	50	0.480	40
S55	1.068	0.956	0.112	15.252	17.891	1.17	49	55	0.526	40
S60	1.059	0.949	0.110	14.823	17.477	1.18	54	60	0.569	40
S65	1.065	0.955	0.110	15.482	17.868	1.15	58	65	0.621	40
S70	1.055	0.940	0.115	15.242	18.150	1.19	62	70	0.658	40
S80	1.064	0.928	0.136	15.781	18.819	1.19	70	80	0.742	40
S90	1.056	0.907	0.149	15.238	17.853	1.17	77	90	0.816	40
S95	1.069	0.920	0.149	15.099	17.390	1.15	82	95	0.874	40
S100	1.059	0.920	0.139	15.306	18.336	1.20	87	100	0.920	40
S00-25	1.060	1.0505	0.009	15.108	15.579	1.03	0	0	0.000	25
S50-25	1.066	1.0223	0.043	14.995	15.606	1.04	50	50	0.511	25
CV100	1.061	–	–	15.231	–	–	–	–	–	–

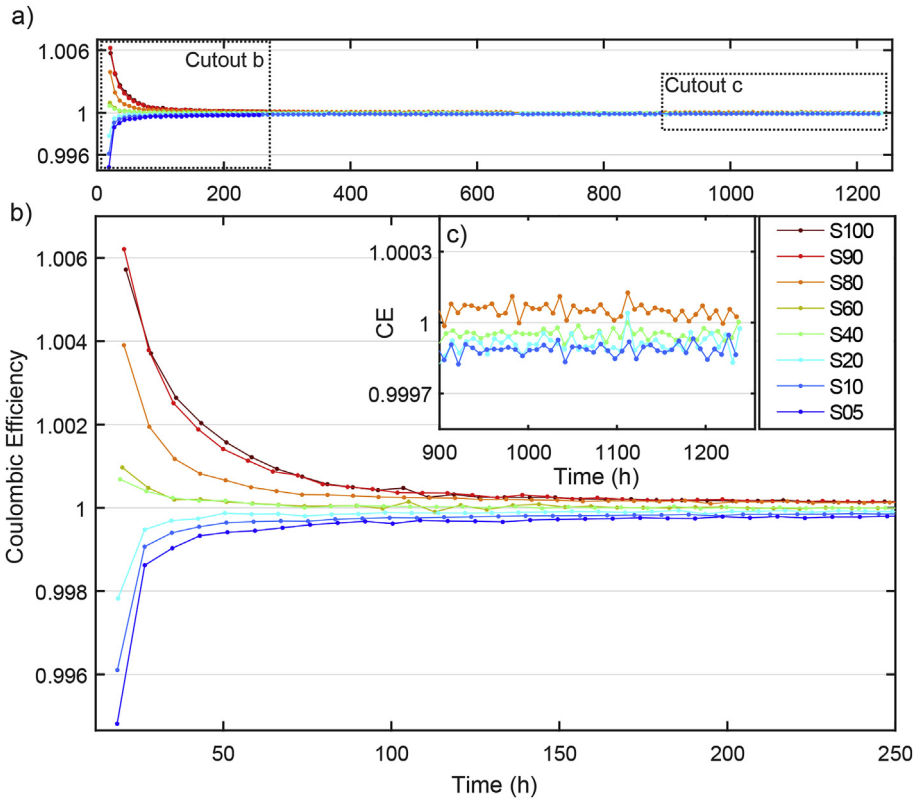

Fig. 3. Coulombic efficiency during cycling after storage for 20 months at various SoC. The data up to 1200 h of cycling is shown in a). b) shows a close up of the initial 30 cycles. c) Cycling was continued for S05, S20, S40 and S80 for 1200 h until all samples showed a narrow range of CE.

discharging than is inserted during charging. This can also be seen in Fig. 4 a), where the charging and discharging capacities are shown for the first 30 cycles.

The batteries stored at low SoC 5%, 10%, and 20% with CE values lower than unity feature decreasing capacities throughout the cycling procedure. Fig. 3 b) shows that initial CE values range from 0.994 to 0.996 for low SoC storage cells and increase successively towards 1. The batteries stored at medium SoC of 40% and 60% consistently show CE values close to 1 and little capacity change during 250 cycles as seen for cell S40 in Fig. 4 b).

These observations are consistent with the observations by Gyenes et al. [16] and can be explained by lithium diffusion into and out of the overhang areas. During long term storage at high SoC, lithium diffuses into the overhang area. During subsequent cycling, the overhang areas act as a lithium source and increases the amount of cyclable lithium. This effect results in a capacity increase of the battery and a CE > 1. After low SoC storage the reverse process occurs. When storing cells at low SoCs, the overhang areas remain largely non-lithiated. During subsequent cycling, the empty overhang areas act as lithium sinks and decrease the amount of cyclable lithium when the average SoC during cycling is higher than the SoC during storage. The corresponding difference in the anode potential drives lithium diffusion into the overhang areas and leads to CE < 1.

After about 30 cycles the cycling procedure was interrupted for cells S10, S60, S90 and S100 when they were in a discharged state, as the cells were disassembled for post-mortem analysis. For the other four cells S05, S20, S40 and S80 cycling was continued for 1200 h before disassembly. As shown in the inlet (Fig. 3 c)), after 1200 h of cycling battery S80 continues to show a CE > 1 and slightly than S05, S20 and S40. This was unexpected as based on Gyenes et al. [16] we expected the CE to drop below 1 after approximately 800 h. As a consequence, we restarted the cycling procedure and continued it up to 300 cycles (2000 h). The time the cells spent at low SoC during the interruption of the cycling procedure led to a certain acceleration of the overhang depletion of cell S80, as can be seen in Fig. 4 b). Sample S80 shows a capacity increase of 2.0% (22 mAh) after 250 cycles, 1.3% (14 mAh) during the initial 30 cycles. Vice versa, Fig. 4 b) shows a capacity decrease of cell S05 by 1.6% (18 mAh) after 250 cycles, 0.5% (5 mAh) after the initial 30 cycles. The capacity difference between S80 and S05 reduces from 6.9% C_N measured directly after storage to 3.3% C_N after 250 cycles, corresponding to 2000 h of cycling. Thus, the 40 mAh difference (3.6% with respect to the nominal capacity) between these measurements is not caused by aging effects, but a result from lithium outflow of overhang areas for cell S80 and lithium inflow into overhang areas for cell S05.

In many battery aging studies, the end of life is considered as a capacity fade of 20% of the nominal capacity. Therefore, variations of 3–4% in the capacity determination caused by the anode overhang areas can lead to substantial misinterpretations of battery aging processes distorted battery life estimations. Applying this 20% capacity fade limit, the end of life is reached at a remaining capacity of 880 mAh. The combined capacity difference of 40 mAh attributed to overhang area effects amounts to 18% of the useable capacity range (220 mAh).

3.3. Post-mortem analyses

The CE observations can be consistently explained by lithium diffusion into the anode overhang areas. To obtain more detailed information about the spatial lithium distribution, post-mortem analyses were performed. The surface color distribution and XRD measurements are evaluated to determine local lithium

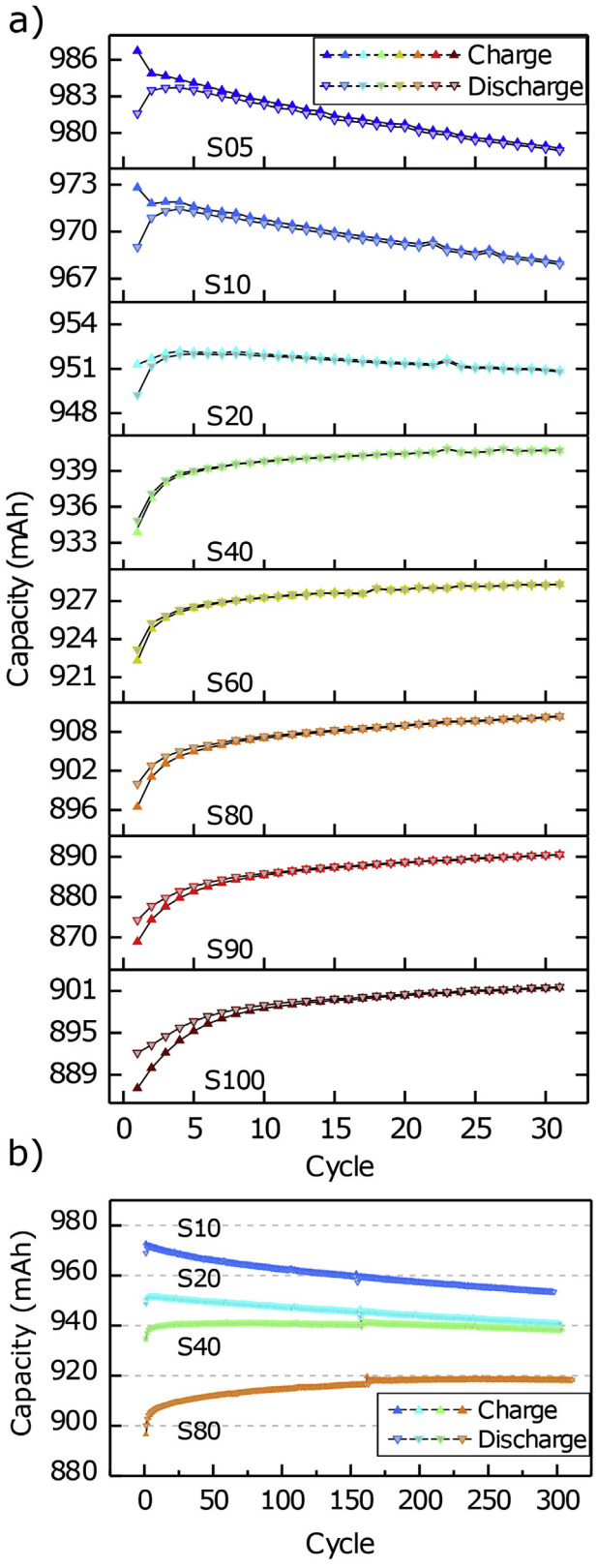

Fig. 4. a) Charging and discharging capacity during the initial 30 cycles (250 h) after long term storage at different SoCs ranging from 5% to 100%. This demonstrates the capacity recovery for cells which exhibit CE values greater than 1. b) Extended cycling data of cells S10, S20, S40 and S80 comprising of up to 300 cycles (2400 h). Discontinuance and restart of the cycling procedure at cycle 160.

concentrations.

3.3.1. Overhang lithiation after storage

After long-term storage at high SoC, considerable amounts of lithium can be found in the anode overhang regions. As the highest amounts of lithium are stored in the overhang areas for the cells which were stored at high SoC, the cell S95 was disassembled after 20 months of storage at 95% SoC and 40 °C. This cell was not subject to subsequent charge-discharge cycling since this would have altered the lithium content in the overhang areas. Fig. 5 shows the graphite color distribution a) and graphite phase fraction along the length of the electrode b) and across the width of the electrode c) of this cell. The large overhang region at the left side, which represents the outer end of the jelly roll, is of purple color with a radial color gradient towards a light blue central part. The purple color of the overhang region indicates 50% anode lithiation [19]. The brighter blue region indicates lower lithiation of 30–50%. In the cathode covered electrode area, color gradients are visible from purple over purple-brownish to golden. Golden areas indicate highly lithiated graphite with LiC_6 present [19]. The color distribution indicates a SoC gradient along the electrode length where the central areas show the highest lithiation. Close to the sides and edges, where overhang regions are located the active anode shows purple color, and thus a lower SoC compared to golden, highly lithiated, central regions.

In addition to the photographs of the electrode, XRD measurements were performed along the length and along the width of the electrode. The measurement positions are illustrated in the backside images of Fig. 5 a). The lithiation gradients observed in the color distribution are also seen in the diffraction measurements. Fig. 5 b) exhibits for the outermost 6 cm, the overhang area without cathode counterpart, and up to 6 cm into the active region, lithiation with LiC_{12}. This is in agreement to the color distribution. At the center of the overhang area (2–4 cm) ~20% LiC_{18} is observed. This corresponds well to the lighter blue colored region at the center of the overhang region where a reduced lithiation is observed compared to purple colored graphite areas. From 12 cm towards the center of the electrode, LiC_6 is present in increasing and then stable amounts of 25%. Along the width of the electrode (Fig. 5 c)) a similar gradient is visible. While only LiC_{12} is present close to the sides, the amount of LiC_6 increases towards the center and plateaus at 25%. The slight asymmetry in lithiation with regard to the center (2.9 cm width) is equally present in the color map and phase distribution as determined by XRD. The approximately 1 cm^2 large area of the anode with the cathode current collector tab as counterpart is recognizable in Fig. 5 a) due to the imprint of the tab and light purple color. The color change and XRD measurement at the central position of this area shows a 100% LiC_{12} lithiation (see S95-Tab in Tables S7–6 for refinement data). Thus, the anode parts opposed to the cathode tab act as source and sink similar to anode overhang areas.

In summary, color distribution and XRD data show lithiation of overhang areas and strong gradients from electrode sides and edges towards the central areas. From the pattern of lithiation seen in Fig. 5, we can draw conclusions on the transport process driving the lithiation of the overhang area. If the process was driven by diffusion through the active material, we would expect the lithiation of the large 6 cm overhang area coming solely from the adjacent active anode area on the right side. A phase boundary parallel to the active area boundary would have to emerge. Yet, the overhang is lithated concentrically from all sides of the electrode, including side areas without direct contact to active anode area.

Thus we conclude that electrochemical processes effect the lithiation of the overhang areas: Lithium ions from the electrolyte intercalate into the overhang graphite material. Simultaneously,

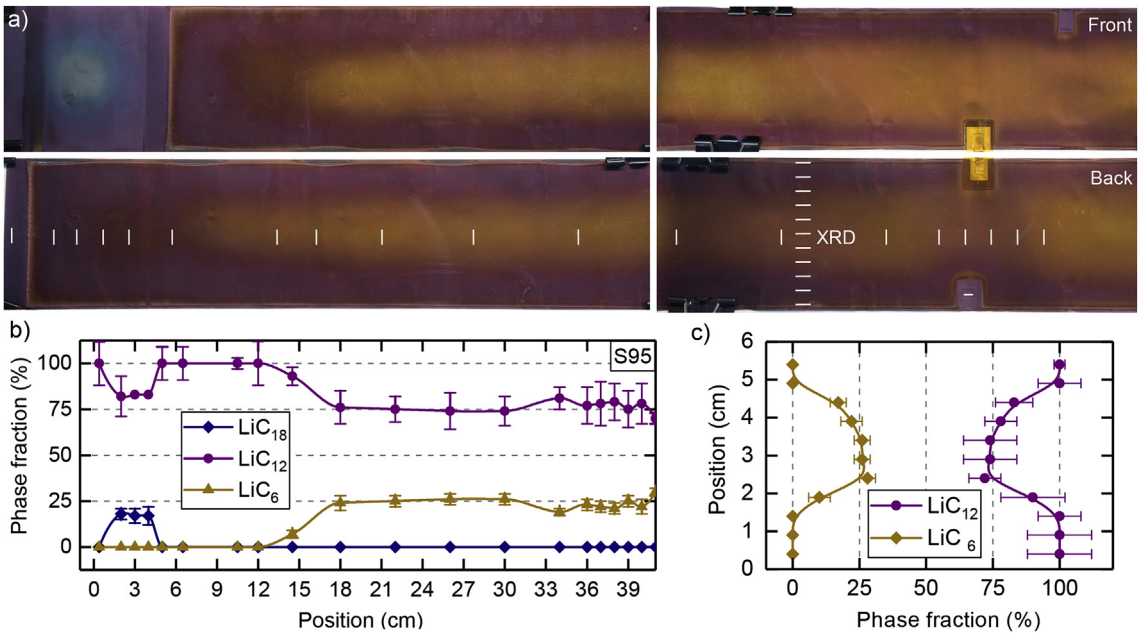

Fig. 5. a) Anode of sample S95 stored at 95% SoC including the overhang region up to the central tab. Varying degrees of graphite lithiation cause an inhomogeneous purple/golden color distribution. b) LiC_x phase fraction determined by Rietveld refinement from XRD measurements along the anode as marked in white on the backside image. c) LiC_x phase fraction across the electrode width. (For interpretation of the references to colour in this figure legend, the reader is referred to the web version of this article.)

lithium from the active graphite area deintercalates. The resulting concentration gradient in the electrolyte equilibrates through liquid diffusion. We consider the potential gradient between differently lithiated anode areas as the main driver for the overhang lithiation. We expect higher temperatures to accelerate the lithiation of the overhang areas by reducing the charge transfer resistances at the electrode-electrolyte interface [37,38] and increasing the diffusion coefficient of the electrolyte [39].

3.3.2. Overhang lithiation at different storage SoCs

To investigate the SoC dependency of large overhang area lithiation in more detail, we performed post-mortem investigation on two additional cells stored for 20 months at very low SoC (S00) and medium SoC (S55). Fig. 6 shows a comparison of the color distribution and graphite lithiation determined at the overhang area between cell S00, S55 and S95.

The overhang area of S00 is of light grey color and the cathode covered part is of grey-brown color. The XRD measurements show a

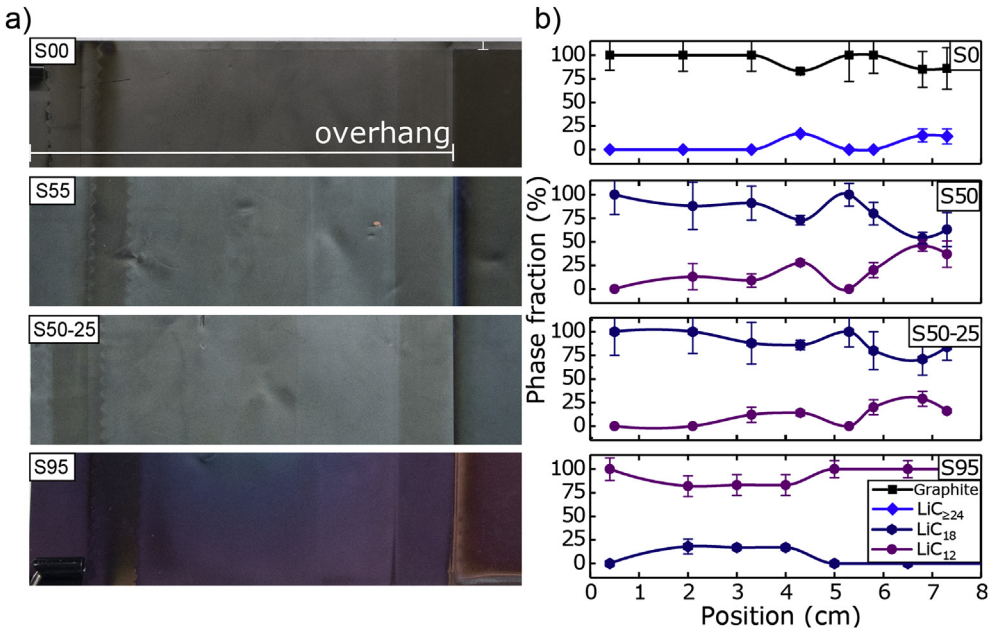

Fig. 6. a) Anode overhang regions for batteries stored at 0%, 50% (25 °C), 55% and 95% SoC along with b) measured LiC_x phase fraction. The presented segments show the upper (S00), middle (S55, S55-25) and lower (S95) part of the overhang area. XRD measurement positions are as shown in Fig. 5. The photographs and phase fractions demonstrate the dependency of the lithiation of the overhang areas on the storage SoC of the lithium-ion cell.

majority of non-lithiated graphite in the overhang as well as at the edge of the active region. Additionally, 0–20% of a slightly lithiated $LiC_{\geq 24}$ phase is observed. The c-parameter of this phase is about 6.80 Å and strongly shifted towards the graphite c-axis parameter of 6.7220(1) Å [30] indicating minimal lithium content. The overhang area is not charged through lithium diffusion, as it is expected for low SoC storage. The remaining contribution of a minimal lithiated phase is consistent with our test procedure that discharges the battery to 2.0 V.

Sample S55 shows a homogeneous grey-blue color with a similarly brighter overhang region. XRD measurements show the overhang regions and active regions lithiated with predominantly LiC_{18} with fractions of higher lithiated LiC_{12} states.

To get a first impression of the temperature dependency of overhang lithiation, we investigated an additional cell S50-25 stored at 50% SoC and 25 °C. Compared to cell S55, this cell shows a similar grey-blue color and also predominantly LiC_{18} lithiated graphite in the overhang area. On average, the share of LiC_{12} is higher for S55 stored at 40 °C (0–46%, avg. 19%) than for S50-25 stored at 25 °C (0–29%, avg. 11%). Lithiation and the according color change, as shown in Fig. 6 is equally present at the 2 cm overhang region at the inner part of the jelly roll (see Supplementary Figs. S3–S14). In conclusion, high storage SoC and elevated temperature are conducive to but not necessary for lithiation of large overhang regions. The common storage SoC of 50% at room temperature is sufficient, given enough storage time, to obtain homogeneously lithiated large overhang areas.

The slight color difference between overhang region and active anode area is visible for all overhang regions, sides and edges, and all samples (See Supplementary Figs. S3–S14 for additional images). We attribute this to a thin passivation layer of the anode, commonly referred to as the solid electrolyte interphase (SEI), which is the dominant aging mechanism of calendar aging in the absence of damaging processes such as mechanical strain and lithium plating during cycle aging [40] [41]. As shown in Fig. 3 c), all cells show capacity loss as expected from passivation layers binding cyclable lithium. The batteries were stored at elevated temperatures which aids the evolution of passivation layers [42]. Klett et al. observed an additional uneven deposition layer on top of the anode for deep cycled $LiFePO_4$|graphite batteries [43,44]. The cycling of the calendar aging batteries was minimal and limited to the check up procedures. Thus, a thick deposition layer as observed by Klett et al. is not thought to be the reason for the observed difference in color. Furthermore, scanning electrode microscope (SEM) images of the overhang area in comparison to active electrode parts (see Supplementary Fig. S2) show a similar surface morphology with no indication of a thick covering layer in both areas.

In addition to the large overhang areas, we investigated the lithiation of the side overhang areas. They are thinner but considerably longer (0.15 cm × 70.2 cm) than the overhang regions at the electrode ends. With the shorter diffusion path, it is expected that the time needed to fill and deplete these areas is short compared to the overhang region at the end of the electrode. Fig. 7 compares the side overhang region of a) S95 with b) S55, c) S00 and a fully charged reference sample d) CV100. Similarly to the large overhang regions, the sides are grey and delithiated for S00, partially lithiated and grey-blue for S55 and purple-red for S95. The side overhang regions take on the state of lithiation of the active region during storage. S00 shows a majority of graphite with a minor contribution of a slightly lithiated $LiC_{\geq 24}$ phase as seen for the large overhang area (Fig. 6). S55 shows a mixture of LiC_{12} and LiC_{18} in with a lower contribution of ~20% LiC_{12} in the side overhang compared to ~50% in the active anode area at position 1 mm and 2 mm. For Cell S95 only LiC_{12} was found in the overhang as well as the active anode area.

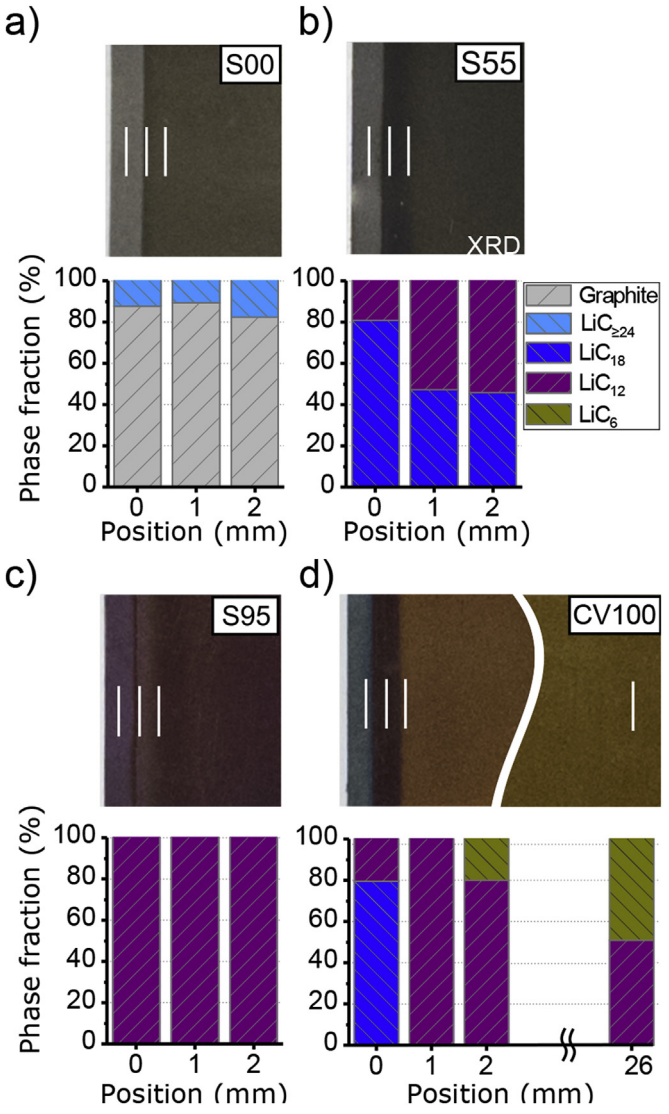

Fig. 7. Close up image of the anode overhang region at the side (1.5 mm) of sample a) S00 b) S55 c) S95 and d) CV100 measured with XRD at three positions, each 1 mm apart. The reference for a fully charged non-aged and non-stored battery CV100 was measured additionally at the central electrode position 26 mm. For the corresponding backside images see Supplementary Figs. S4–14.

To assess the accuracy of the phase identification of XRD, we compare the graphite lithiation obtained through XRD for the fully charged reference cell CV100 with the results of a dV/dQ analysis. The fully charged CV100 cell shows three sharply divided colored 1 mm wide areas, a light blue overhang, a golden highly lithiated area and a partial lithiated purple area in between. Consistent with this, XRD measurements show lower lithiated states LiC_{18} in the blue, LiC_{12} in the purple and LiC_{12}/LiC_6 in the golden region. The LiC_6 fraction in the lithiated region close to the sides (2 mm) is with 20% low compared to the 49% measured at the center of the electrode (26 mm), indicating a reduction in lithium content at least partially due to the diffusion into the overhang. The observed 51% LiC_{12} to 49% LiC_6 ratio at the center is slightly higher than the 57% LiC_{12}/43% LiC_6 average ratio expected from dV/dQ analysis. This can be explained through the inhomogeneous SoC in the active anode area. With a LiC_6 gradient towards the central region, similar to cell S95, the higher than average lithiated areas at the center compensate for the lower than average lithiated areas at the sides.

Thus, XRD and dV/dQ are in good agreement.

3.3.3. Depletion of overhang areas after CE cycling

To investigate qualitatively how quickly the overhang area can be delithiated, we compare the overhang areas between samples after cycling and samples after cycling with additional CCCV discharges at low SoC. Cell S90 was opened directly after discharge after about 30 cycles for CE measurements without additional measures to deplete the overhang area. The cathode covered anode area is delithiated and appears brown-grey (Fig. 8 a)). The grey-blue colored overhang region indicates partial lithiation. This is confirmed by the XRD measurements of the central region which shows 60% ± 25% graphite and 40% ± 15% LiC_{18} (see Fig. 8 a) for measurement position and Supplementary Tables S7–8 for detailed diffraction results). Within the margin of error, we see an even share of LiC_{18} and graphite. There are no lower lithiated phases $LiC_{\geq 24}$ in-between graphite and LiC_{18} present. At the measured position, the back area is not part of the overhang and therefore delithiated during discharge. Thus, the observed 60% graphite are attributed to the back of the electrode.

Light grey colors at the sides and at the overhang in close proximity to the active region indicate delithiation. This is confirmed through XRD measurement of side overhang areas near the middle part of the electrode, which shows mainly graphite and a minor contribution of low lithiated phase $LiC_{\geq 24}$ of 11% ± 5% of a (c-axis = 6.854(7) Å) (see the inlet of Fig. 8 b) and Supplementary Tables S7–8 for detailed diffraction results).

When comparing the two cells S90 and S95 (Fig. 5), which were both stored 20 months at a high SoC, the impact of cycling on the lithiation of the overhang areas becomes obvious. Whereas the cell without cycling exhibits a mixture of LiC_{12} and LiC_{18} phases, the cycled cell only exhibits LiC_{18} phases at the center. Thus, the lower average potential of the active anode area during cycling led to a lithium diffusion from the overhang area back to the active area, which explains the CE > 1 and the capacity increase in the cycling experiment.

3.3.4. Depletion of overhang areas after CE cycling and additional CCCV discharges

In completely discharged condition, the anode potential is highest (see Fig. 1 a)) and the gradient between lithiated overhang areas and the active area is most pronounced. This leads to the fastest diffusion of lithium back to the active area [16]. In order to remove as much lithium as possible from the overhang areas, several cells were CCCV discharged repeatedly. The cells S100, S70, S60 and S05 were taken from the cycling procedure after ca. 30 cycles when they were completely discharged. Subsequently, they were exposed to five CCCV discharges with 10 h of relaxation in between. To accelerate diffusion, the storage and discharge procedure was carried out at 50 °C. After that, the cells were opened and post-mortem studies were performed.

The battery voltage during the five consecutive CCCV discharges with 10 h relaxation as well as the discharged capacity for each step for cell S100, S60 and S05 are shown in Fig. 8 c). The cells show different voltage relaxation behavior, despite identical test procedures. Higher voltage levels are seen during relaxation for higher

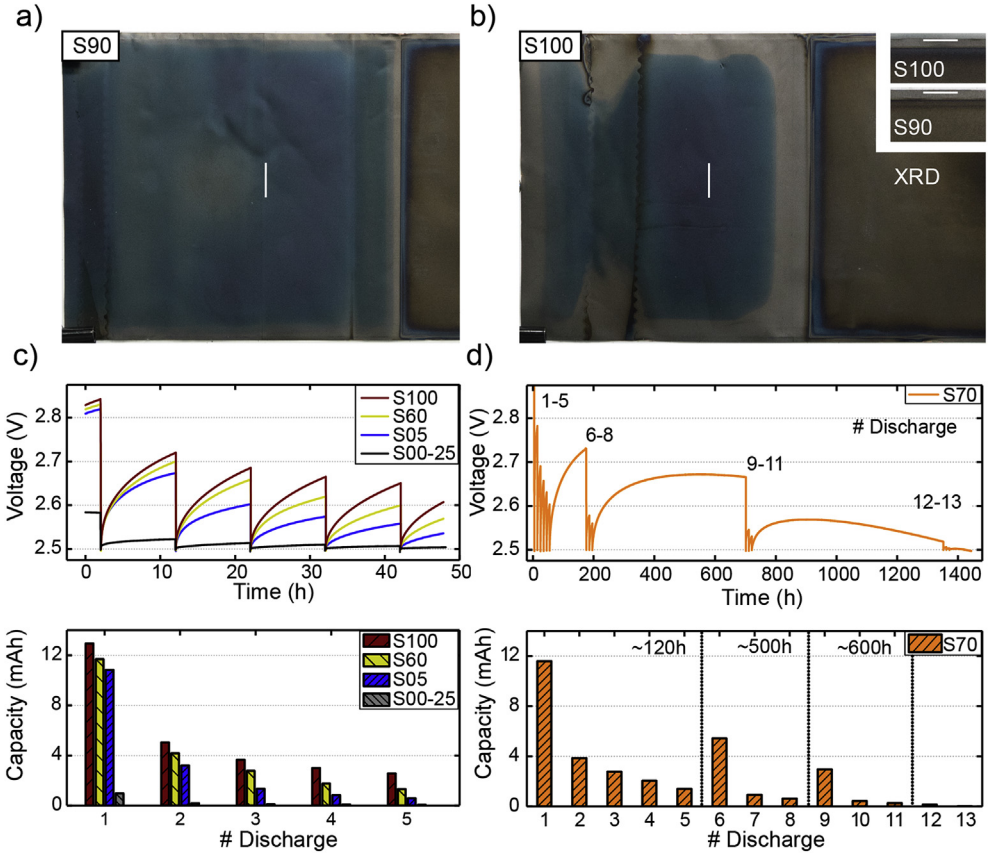

Fig. 8. Anode overhang region for a) S90 and b) S100 after C/4 cycling for 250 h. The inlet shows side overhang regions. S100 additionally underwent five CCCV discharges and 50 h storage at 50 °C. White bars mark the XRD measurement positions. c) Battery voltage of S100, S60, S05 and S0-25 during CCCV discharge and subsequent 10 h relaxation. d) Sample S70 underwent 13 CCCV discharges with subsequent 10 h relaxation. More time was given for relaxation between discharge 5 and 6 (120 h), 8 and 9 (500 h) as well as 11 and 12 (600 h).

storage SoC batteries, due to remaining lithiated areas in the overhang region. The extracted capacity decreases monotonically with the number of discharge steps for all samples. The higher the previous storage SoC the higher is the extracted capacity. The extracted capacity decreases more sharply for the low SoC storage sample S05 (5%) compared to sample S100. For example, at the first discharge ~20% more capacity was extracted for S100 compared to S05 (12.9 mAh compared to 10.8 mAh). At the fifth discharge, four times the capacity was extracted from S100 (2.6 mAh compared to 0.6 mAh).

The effect of the discharge procedure onto the large overhang area is depicted in Fig. 8 b) for the high storage SoC cell S100. As for sample S90, the overhang region shows a blue LiC_{18} lithiated graphite area as confirmed with an XRD measurement of the center area (Fig. 8 b)). Similar to S90 the side overhang areas are delithiated. They are of light grey color and XRD measurements show a majority of graphite and a minor contribution of low lithiated phase $LiC_{\geq 24}$ of 15% ± 8% (c-axis = 6.839(7) Å).

The grey areas observed for S100 after the five CCCV discharges are wider than for S90 (1 cm compared to ~1.5 mm). As the grey areas represent a lower degree of lithiation than the blue areas, it is confirmed that the subsequent discharges and the prolonged storage at low SoC have made lithium diffuse out of the overhang area back to the active area where it became available for discharging again.

Taken together, these results confirm that the increase in capacity and CE > 1 during cycling of high SoC storage cells is caused by lithium influx from the overhang areas. They also show a difference in accessibility of large and small overhang regions. During CE cycling the small overhang regions are largely depleted during each discharge of each cycle at our chosen rate (C/4). This is in agreement with Lewerenz et al., who observed a 2–3% higher capacity for C/4 discharges compared to 1C for a cylindrical LFP|graphite battery and attributed this to the “near part” of the anode overhang [45]. Thus, the withdrawable capacity stems from the larger 2–6 cm wide electrode-edge overhang regions. The rather large amount of capacity extracted from S05 during the first discharge seems to contradict this interpretation (Fig. 8 c)), as one would expect a lower capacity for largely empty overhang areas. The discrepancy can be explained by the following:

First, the higher temperature during the depletion procedure at 50 °C compared to 25 °C during CE cycling frees additional capacity in the active anode area. Secondly, as suggested by Gyenes et al. [16], the overhang areas asymptotically approach the medium SoC of the cycling procedure, which is 50% for full range cycling applied in the CE measurements.

To verify the second assumption, a cell stored at 0%, S00-25 without prior cycling, was also exposed to the described depletion procedure. For this cell, it was expected that almost no lithium is stored in the overhang areas. Thus, no charge extraction and voltage recovery should occur for this cell. As can be seen in Fig. 8 c), only a very minor amount of charge could be discharged for this cell and the voltage recovery is also small. The assumption is further supported by post-mortem investigation of sample S80, S40, S20 and S10 after the CE measurements. All four samples show slightly grey-blue colored, partially lithiated large overhang areas (see Supplementary Figs. S6, S9, S10, S11).

As there was still a considerable voltage recovery after five CCCV discharges, another cell, S70 underwent an extension of the procedure for the three cells discussed above, with longer storage and more discharges. Fig. 8 d) shows that there is a voltage recovery observable for almost 1000 h. Moreover, the amount of extractable charge increases with longer rest periods at 0% SoC. In total, about 32.5 mAh could be extracted during the 13 subsequent CCCV discharge steps. This amount of charge represents 3.0% C_N and can be considered as the full amount of charge stored in the large overhang area of the anode for this cell.

4. Conclusion

Anode overhang assures 100% overlap between the electrodes and is thus a common feature in lithium-ion battery cell design. To study overhang lithiation, we evaluated 16 batteries stored at 40 °C and 0%–100% SoC as part of a preceding calendar aging study.

The overhang areas and thus their lithium storage capability can be considerable and non-negligible compared to full battery capacity. The 18650 $LiFePO_4$|graphite battery examined in this study has overhang areas of 10% of the total anode area. The share of overhang area is approximately evenly split between 2 cm and 6 cm wide sections at the outermost and innermost part of the jelly roll and 1.5 mm thin stripes at the top and bottom of the electrode extending over the full anode length.

By color assessment and x-ray diffraction measurements, we show that thin overhang stretches as well as large overhang areas can be lithiated during long term storage. Overhang areas after storage at high SoC, show LiC_{12} lithiation and a graphite color change to purple-red. After storage at or operation at medium SoC, mainly LiC_{18} lithiation and a graphite color change to grey-blue is observed. Little difference in overhang lithiation was seen between medium storage SoC batteries stored for 20 months at 40 °C and 25 °C. As expected, no increased lithiation of overhang areas was found at low SoC storage. In conclusion, high storage SoC and elevated temperature are conducive to, but room temperature and medium SoC are sufficient for, lithiation of large overhang regions.

We observe a distinct difference in perceived brightness between anode overhang and active area independent of lithiation consistently for all calendar aged cells. We attribute this to differences in graphite passivation layers, the origin of which is not fully understood. Despite this, we find good agreement between the qualitative observations through color and quantitative measurements of the graphite phase fractions with XRD. Thus, our results support the validity of graphite color changes as qualitative measure of overhang lithiation as applied in this and previous work about anode overhang areas.

We find the lithiated overhang areas strongly affect capacity and CE measurements. For high SoC storage batteries, CE > 1 and successively increasing capacity is observed for more than 1200 h of cycling (50 days) as lithium diffuses out of the overhang area, longer than previously reported. Vice versa, empty overhang regions after storage at low SoC lithiate during cycling causing CE < 1 and a disproportionately decreasing capacity. Consequently, the storage history must be considered in the analysis of high precision CE measurements if excess anode area is present.

Furthermore, our tests show that SoH assessment for calendar aged batteries can be flawed if batteries are compared with tests conducted directly after long term storage at varying SoC. We found a 6.9% C_N capacity difference between a low and high storage SoC battery to narrow down to 3.3% C_N after cycling. We attribute these long term effects predominantly to large overhang areas and not few millimeter thin side areas, as discharged batteries show grey colored depleted side areas after a few cycles compared to blue colored LiC_{18} lithiated large overhang areas.

To reduce the reversible capacity effect and the resulting storage history dependence, the cell design of a cylindrical cell needs to avoid the large overhang areas at the outermost or innermost part of the jelly roll, for example, by not coating this area.

The observed effects are not limited to commercial battery cells, but are also expected to be present in laboratory cells, in particular, under the assumption that manually crafted cells use large overhang areas to compensate for the lack of machine precision in

electrode positioning. Further analysis of the speed of lateral lithium propagation could help to understand how quickly overhang areas of differing sizes are lithiated and how to minimize their impact on CE and SoH determination for any given battery design.

Acknowledgments

The German Federal Ministry of Education and Research (BMBF) financially supports this work under grant number 03XP0081 (ExZellTUM II). The authors thank Prof. Hubert Gasteiger for granting access to glovebox laboratory equipment and the Heinz Maier-Leibnitz Zentrum for access to the Materials Science Laboratory.

Appendix A. Supplementary data

Supplementary data related to this article can be found at http://dx.doi.org/10.1016/j.jpowsour.2017.08.090.

References

[1] A. Barré, B. Deguilhem, S. Grolleau, M. Gérard, F. Suard, D. Riu, J. Power Sources 241 (2013) 680–689.
[2] J. Zhang, J. Lee, J. Power Sources 196 (2011) 6007–6014.
[3] P. Keil, S.F. Schuster, J. Wilhelm, J. Travi, A. Hauser, R.C. Karl, A. Jossen, J. Electrochem. Soc. 163 (2016) A1872–A1880.
[4] J. Belt, V. Utgikar, I. Bloom, J. Power Sources 196 (2011) 10213–10221.
[5] S. Grolleau, A. Delaille, H. Gualous, P. Gyan, R. Revel, J. Bernard, E. Redondo-Iglesias, J. Peter, J. Power Sources 255 (2014) 450–458.
[6] S. Käbitz, J.B. Gerschler, M. Ecker, Y. Yurdagel, B. Emmermacher, D. André, T. Mitsch, D.U. Sauer, J. Power Sources 239 (2013) 572–583.
[7] M. Kassem, J. Bernard, R. Revel, S. Pélissier, F. Duclaud, C. Delacourt, J. Power Sources 208 (2012) 296–305.
[8] I. Bloom, B. Cole, J. Sohn, S. Jones, E. Polzin, V. Battaglia, G. Henriksen, C. Motloch, R. Richardson, T. Unkelhaeuser, D. Ingersoll, H. Case, J. Power Sources 101 (2001) 238–247.
[9] M. Ecker, N. Nieto, S. Käbitz, J. Schmalstieg, H. Blanke, A. Warnecke, D.U. Sauer, J. Power Sources 248 (2014) 839–851.
[10] M. Safari, C. Delacourt, J. Electrochem. Soc. 158 (2011) A1123.
[11] S.B. Peterson, J. Apt, J.F. Whitacre, J. Power Sources 195 (2010) 2385–2392.
[12] A.J. Smith, J.C. Burns, J.R. Dahn, Electrochem. Solid-State Lett. 13 (2010) A177.
[13] A.J. Smith, J.C. Burns, D. Xiong, J.R. Dahn, J. Electrochem. Soc. 158 (2011) A1136.
[14] A.J. Smith, J.C. Burns, S. Trussler, J.R. Dahn, J. Electrochem. Soc. 157 (2010) A196.
[15] J.C. Burns, G. Jain, A.J. Smith, K.W. Eberman, E. Scott, J.P. Gardner, J.R. Dahn, J. Electrochem. Soc. 158 (2011) A255.
[16] B. Gyenes, D.A. Stevens, V.L. Chevrier, J.R. Dahn, J. Electrochem. Soc. 162 (2014) A278–A283.
[17] M. Tang, P. Albertus, J. Newman, J. Electrochem. Soc. 156 (2009) A390.
[18] M. Lewerenz, J. Münnix, J. Schmalstieg, S. Käbitz, M. Knips, D.U. Sauer, J. Power Sources 345 (2017) 254–263.
[19] P. Maire, A. Evans, H. Kaiser, W. Scheifele, P. Novák, J. Electrochem. Soc. 155 (2008) A862.
[20] S.J. Harris, A. Timmons, D.R. Baker, C. Monroe, Chem. Phys. Lett. 485 (2010) 265–274.
[21] D. Manka, E. Ivers-Tiffée, Electrochimica Acta 186 (2015) 642–653.
[22] J. Liu, M. Kunz, K. Chen, N. Tamura, T.J. Richardson, J. Phys. Chem. Lett. 1 (2010) 2120–2123.
[23] T.M. Bond, J.C. Burns, D.A. Stevens, H.M. Dahn, J.R. Dahn, J. Electrochem. Soc. 160 (2013) A521–A527.
[24] T. Degen, M. Sadki, E. Bron, U. König, G. Nénert, Powder Diffr. 29 (2014) S13–S18.
[25] P. Thompson, D.E. Cox, J.B. Hastings, J. Appl. Crystallogr. 20 (1987) 79–83.
[26] H.M. Rietveld, J. Appl. Crystallogr. 2 (1969) 65–71.
[27] G.S. Pawley, J. Appl. Crystallogr. 14 (1981) 357–361.
[28] A.S. Cooper, Acta Cryst. 15 (1962) 578–582.
[29] H.M. Otte, J. Appl. Phys. 32 (1961) 1536–1546.
[30] O. Dolotko, A. Senyshyn, M.J. Muhlbauer, K. Nikolowski, F. Scheiba, H. Ehrenberg, J. Electrochem. Soc. 159 (2012) A2082–A2088.
[31] D. Guerard, A. Herold, Carbon 13 (1975) 337–345.
[32] B. Vadlamani, K. An, M. Jagannathan, K.S.R. Chandran, J. Electrochem. Soc. 161 (2014) A1731–A1741.
[33] D. Billaud, F.X. Henry, M. Lelaurain, P. Willmann, J. Phys. Chem. Solids 57 (1996) 775–781.
[34] M. Heß, P. Novák, Electrochimica Acta 106 (2013) 149–158.
[35] S. Taminato, M. Yonemura, S. Shiotani, T. Kamiyama, S. Torii, M. Nagao, Y. Ishikawa, K. Mori, T. Fukunaga, Y. Onodera, T. Naka, M. Morishima, Y. Ukyo, D.S. Adipranoto, H. Arai, Y. Uchimoto, Z. Ogumi, K. Suzuki, M. Hirayama, R. Kanno, Sci. Rep. 6 (2016) 28843.
[36] A. Senyshyn, O. Dolotko, M.J. Muhlbauer, K. Nikolowski, H. Fuess, H. Ehrenberg, J. Electrochem. Soc. 160 (2013) A3198–A3205.
[37] W. Waag, S. Käbitz, D.U. Sauer, Appl. Energy 102 (2013) 885–897.
[38] S.S. Zhang, K. Xu, T.R. Jow, J. Power Sources 115 (2003) 137–140.
[39] L.O. Valøen, J.N. Reimers, J. Electrochem. Soc. 152 (2005) A882.
[40] P.B. Balbuena, Y. Wang, Lithium-ion Batteries: Solid-electrolyte Interphase, Imperial College Press, London, 2004.
[41] S.-P. Kim, A.C. van Duin, V.B. Shenoy, J. Power Sources 196 (2011) 8590–8597.
[42] J. Vetter, P. Novák, M.R. Wagner, C. Veit, K.-C. Möller, J.O. Besenhard, M. Winter, M. Wohlfahrt-Mehrens, C. Vogler, A. Hammouche, J. Power Sources 147 (2005) 269–281.
[43] M. Klett, R. Eriksson, J. Groot, P. Svens, K. Ciosek Högström, R.W. Lindström, H. Berg, T. Gustafson, G. Lindbergh, K. Edström, J. Power Sources 257 (2014) 126–137.
[44] M. Klett, P. Svens, C. Tengstedt, A. Seyeux, J. Światowska, G. Lindbergh, R. Wreland Lindström, J. Phys. Chem. C 119 (2015) 90–100.
[45] M. Lewerenz, A. Warnecke, D.U. Sauer, J. Power Sources 354 (2017) 157–166.